PAPER • OPEN ACCESS

Low Cycle Fatigue Properties of Aluminizing Coating on Cold-Drawn AISI 1018 Steel

To cite this article: M Badaruddin *et al* 2020 *IOP Conf. Ser.: Mater. Sci. Eng.* **807** 012019

View the article online for updates and enhancements.

Low Cycle Fatigue Properties of Aluminizing Coating on Cold-Drawn AISI 1018 Steel

M Badaruddin[1]***, R D Kurniawan**[1]**, Sugiyanto**[1]**, A Pambudi**[2]

[1] Department of Mechanical Engineering, Faculty of Engineering, Universitas Lampung, Bandar Lampung, 35145, Indonesia
[2] Department of Mechanical Engineering, Faculty of Engineering, Universitas Malahayati, Bandar Lampung, 35144, Indonesia

*Corresponding e-mail: mbruddin@eng.unila.ac.id

Abstract. The mechanical and the low cycle fatigue (LCF) properties of cold-drawn AISI 1018 steel (CDS 1018) with and without hot-dip aluminizing (HDA) coating had been experimentally investigated at room temperature. The tensile properties and the LCF properties were determined from tensile test results and cyclic strain-fatigue test results, respectively. The aluminide coating on the CDS 1018 significantly decreases the mechanical properties and the strain-fatigue life of the steel. With increasing in strain amplitude levels, CDS 1018 experienced continuously cyclic softening behaviour after cyclic loading in few cycles. By contrast, the cyclic softening of HDA steel was observed in few cycles and HDA steel continuously exhibits the stably cyclic hardening behaviour until failure. CDS 1018 with aluminide coating results the longer transition fatigue cycles (N_t) than those of CDS 1018 without aluminide coating by a factor of ~3.0. CDS 1018 with HDA coating can be used for material components which the components are safely designed under cyclic loading below the yield strength of the material.

1. Introduction

A low carbon steel (mild steel) price is relatively cheaper than those of high alloy steel grades and stainless-steel grades prices, however mild steel properties are acceptable for many applications in engineering component structures. Therefore, mild steel used for the high temperature material components such as a fire piping of boiler, incinerators and heat exchanger should be protected against high temperature oxidation attack via the hot-dipping aluminizing (HDA) coating. It is well known that the aluminide coating on the steel significantly improve the oxidation resistance at elevated temperatures in air and mixtures of steam environments [1−3] and hot corrosion containing of chloride and sulphur environments [4]. Aluminide layer consisting of the Fe_2Al_5 layer on the steel substrate can supply continuously the aluminium atoms to form the protective aluminium oxide (Al_2O_3) layer. During applications, the material can experience plastic deformation due to strain cyclic loading at starting-up

and shut-down periods [5]. Plastic deformation induced the material can cause the component failure in few cycles.

An investigation of an aluminide coating impact on the strength and the fatigue life of steel is very important to determine an initial safety design for engineering components when the aluminized steel products are used for high temperature applications. Aguero et al. reported that the aluminide coating deposited on P91 and P92 steel resulted good ductility of these alloys during creep testing at 650 °C and a small reduction of creep strength was mainly attributable to the presence of voids in the diffusion zone because of formation of Fe-Al intermetallic layer [6]. Furthermore, an aluminizing coating applied on K403 superalloy blades resulted detrimental effect of the fatigue property of the alloy, but the alloy was capable to resist the oxidation attack at 950 °C [7]. Moreover, many voids formed in Fe- and Ni-Al intermetallic layer due to the interdiffusion process lead to rapid degradation of mechanical strength of steel and nickel alloy with aluminide coating [8]. Badaruddin et al [9]. reported that a significant decrease in the mechanical properties of a high strength AISI P20 steel was caused by both the formation of the brittle Fe_2Al_5 layer and voids as results of inter-diffusional process between Fe-atoms and Al atoms in the alloy.

In the present experiments, we focused on an investigation of the low cycle fatigue performance of cold-drawn AISI 1018 steel which was coated by the HDA coating. Few publications are available in literature, reporting the LCF properties of steel with aluminide coating. Therefore, it is important to clarify the impact of aluminide layer on the LCF properties of steel. The CDS 1018 with and without an aluminide coating were fatigued under strain cyclic loading and LCF test results obtained were used to determine the LCF properties using the Basquin and the Coffin-Manson approaches. The empirical equations consisting of combination elastic and plastics terms can be used to predict the fatigue life of the steel for the components in engineering applications where the plastic deformation considerably affects the steel properties.

2. Experimental procedure

2.1. Material and preparation of specimen

A commercial AISI 1018 steel under cold-drawn conditions was used in the present study which its chemical composition was similar with that of the previous research [10]. The tensile and the LCF specimens were provided regarding to ASTM standard E8 [11] and ASTM standard E606 [12], respectively. The tensile and the LCF specimens are shown in Fig. 1a and b, respectively. Details of the procedures for HDA coating process were similar with that of the HDA coating for mild steel in Ref. [4]. The specimen with and without aluminide coating is represented as the HDA steel and the CDS 1018, respectively.
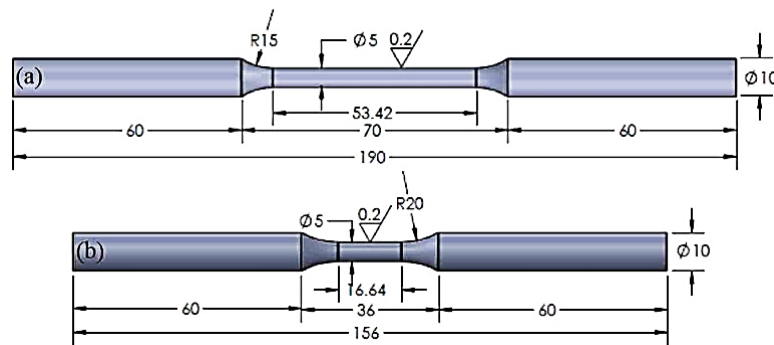
Figure 1. (a) Dimensions of the tensile specimen and (b) the LCF specimen (all in mm)

2.2. Tensile and LCF tests

A servo-hydraulic MTS Landmark test system was used in the present experiments for determining the mechanical properties and the LCF properties of CDS 1018 and HDA steel at room temperature. An MTS model 632.25F-24 axial extensometer with a gauge length of 50 mm was used to measure axial strain during tensile testing at a constant displacement rate of 0.2 mm/min. The mechanical properties for CDS 1018 and HDA steel were determined from the stress-strain curve obtained from the respective three specimens and the typical plot of stress versus axial deformation relationship curve is constructed in Figure 2.

In the present LCF tests, the respective three specimens for CDS 1018 and HDA steel were performed under a fully reversed ramp wave loading controlled by an axial extensometer of MTS 623.12F-20 type under various strain amplitude of 0.003–0.007 mm/mm at constant strain rate of 0.005 s^{-1} with a strain ratio, R = $\varepsilon_{min}/\varepsilon_{max}$ = −1, the frequencies were calculated using the equation in Ref. [13], which a 0.417 Hz, 0.25 Hz, 0.179 Hz were for a strain amplitude of 0.003, 0.005 and 0.007 mm/mm, respectively. During LCF testing, the failure cycles of the specimen was automatically determined when a cyclic loading decreased to a 50% of stable loading cycles [12]. LCF test results consist of plastic strain, elastic strain and elastic modulus data at half cycles (0.5N_f). Pairs data point consisting of plastic strain and elastic strain with reversals to failure cycles (2N_f) at any strain amplitudes were plotted for determining the LCF properties using the Basquin and the Coffin-Manson equations [12].
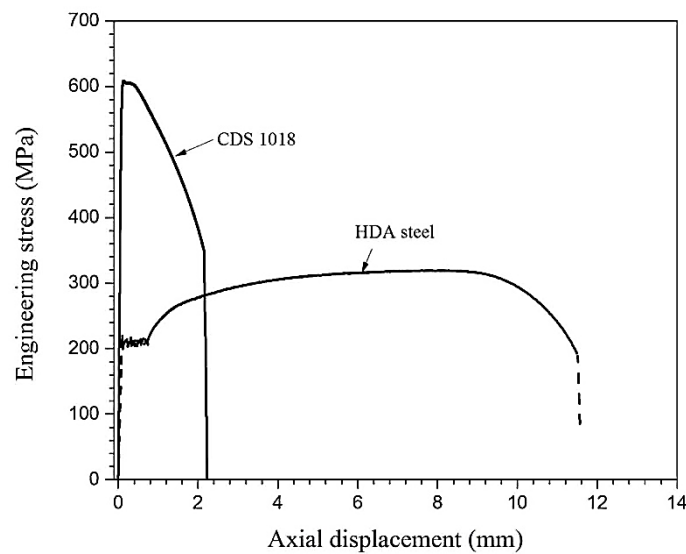
Figure 2. The typical stress-axial displacement relationship
curve for CDS 1018 and HDA steel

Table 1. The average of the tensile properties for CDS 1018 and HDA steel

Property	Material	
	CDS 1018	HDA steel
Elastic modulus (GPa)	210.70	209.82
Yield strength, YS – 0.2% proof stress (MPa)	545	229
Ultimate tensile strength, UTS (MPa)	608	329
Percentage of elongation, e (%)	8.64	46.12
UTS: YS	1.12	1.44

3. Results and discussion

3.1. Tensile test and LCF test results

Figure 2 displays the stress versus axial displacement curve for CDS 1018 and HDA steel. The tensile
properties of the CDS 1018 and the HDA steel are presented in Table 1. Table 2 summarizes the LCF
test results at different strain amplitudes. As shown in Figure 2, CDS 1018 does not show well-defined
yield strength point, which a typical characteristic of mild steel due to cold-drawing process [10]. In
addition, CDS 1018 exhibits a linear plastic behaviour, which can be observed in the region between
yield point and ultimate point (Figure 2). Aluminide coating formed on the CDS 1018 substrate resulted
significant changes in the steel properties: the tensile strength decreased, and the ductility increased. It
could be observed in Figure 2 that CDS 1018 with aluminide coating experienced stress relieving after
aluminizing process. Consequently, the yield points for the HDA steel show clearly a similar
characteristic of low carbon steel [14] and high strength low alloy AISI 4140 steel under annealing
condition [13].

Table 2. LCF test results for CDS 1018 and HDA steel

Specimen	$\Delta\varepsilon_t$ (mm/mm)	ε_a (mm/mm)		E (GPa)	N_f (cycles)
		ε_{ap}	ε_{ae}		
CDS1	0.003	0.00120	0.00180	192.98	7795
CDS2	0.005	0.00305	0.00195	188.90	3980
CDS3	0.007	0.00495	0.00205	191.32	1927
HDA1	0.003	0.00180	0.00120	199.60	6278
HDA2	0.005	0.00341	0.00159	201.57	2085
HDA3	0.007	0.00517	0.00183	191.38	1401

The materials capacity for undergoing strain hardening during monotonic deformation or hardening/softening during fatigue cyclic deformation can be predicted from a value of UTS:YS ratio [15]. The calculated UTS:YS ratio as shown in Table 1 for the CDS 1018 and the HDA steel are an approximately 1.12 and 1.44 respectively. Hypothetically, metallic alloys with UTS:YS ratio lower than 1.2 tend to exhibit cyclic softening behaviour. Conversely, the materials with the UTS:YS ratio > 1.4 generally tend to undergo cyclic hardening behaviour during cyclic loading [13].
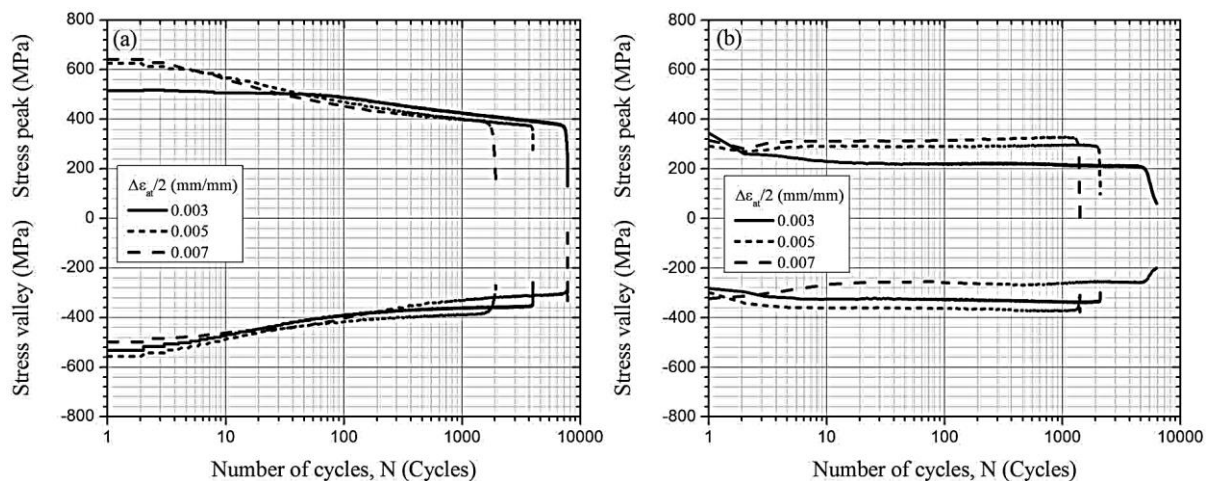

Figure 3. The cyclic stress responses of (a) CDS 1018 and (b) HDA steel with respect to the number of cycles at different strain amplitudes

3.2. Cyclic stress response with respect to fatigue cycles
The cyclic stress responses with the number of cycles at different strain amplitudes for CDS 1018 and HDA steel are displayed in Fig. 3a and b, respectively. The stress peak responses for CDS 1018 steel increase with increasing in strain amplitude levels (Figure 3a). In contrast, HDA steel exhibits a higher

peak stress response at lower strain amplitude (Figure 3b). At a strain amplitude of 0.003 mm/mm, the difference of cyclic stress responses in peak stress (tension) and valley stress (compressive) subjected to the HDA1 specimen is about 170 MPa compared to that of the CDS1 specimen. The CDS1 specimen showed slowly cyclic softening in a loading cycle ranging from 3 to 46 cycles and progressively cyclic softening until failure. Furthermore, as shown in Figure 3a when the strain amplitude was increased to 0.005 and 0.007 mm/mm, CDS 1018 exhibited stably cyclic hardening behaviour in few cycles and continuously cyclic softening behaviour until failure. By increasing in fatigue cycles loading at any given strain amplitude, the CDS specimens undergo cyclic softening behaviour, which can be apparently observed via a gradual decrease in a peak stress (Figure 3a). CDS 1018 experienced continuously cyclic softening behaviour, indicating that an AISI 1018 steel under cold-drawn condition is not capable to cyclically plastic deformation, which is a similar cyclic softening behaviours of SAE 1010 steel in cold-rolled condition [16]. High strain hardening induced AISI 1018 steel after cold-drawing processing decreased significantly plastic deformation capacity [11], which lead to continuously cyclic softening behaviours during strain-controlled fatigue. The softening behaviours of CDS 1018 under low cycle fatigue conditions is evidenced in Figure 3a.

Figure 3b shows that the stress peak responses of the HDA steel specimens rapidly decrease at the 2nd loading cycles. Furthermore, at a strain amplitude of 0.003 mm/mm the HDA1 specimen exhibited gradually cyclic softening behaviours in loading cycle ranging from 3 to 46 cycles, and continually underwent stable cyclic hardening for 4527 cycles. The initiation crack started growing at 5292 cycles and cracks propagated rapidly in the HDA1 specimen which could be indicated by a drastic decrease in the stress peak until fail for 6277 cycles. When the strain amplitude was increased to 0.005 and 0.007 mm/mm, the HDA steel underwent stably cyclic hardening starting from the 8th loading cycles until fail. The initiation cracks for the HDA2 and HDA3 specimens respectively grew at 2057 cycles and 1376 cycles. With increasing in strain amplitude levels, the magnitude of compressive stress in the HDA steel observed in Figure 3b increased gradually with respect to fatigue cycles. The higher valley stress in HDA steel compared to those of the peak stress during strain-fatigue loading indicates that strain hardening induced in the material as result of an increase in dislocation density.

Low dislocation interactions possibly result the cyclic softening in few cycles for the HDA steel (Figure 3b) and the dislocations interaction after few loading cycles is responsible to subsequent stable hardening behaviours. Softening has been observed in cyclic deformation of many alloys, which is generally attributed to the rearrangement of dislocations [16,17]. On the other hand, an increase in dislocation density due to multiplication and interaction among dislocation connections resulted by plastic deformation is strongly responsible to the cyclic hardening behaviours of material. In general, an increase in dislocation density and stronger interaction among dislocations results work hardening during cyclic deformation [13]. Work hardening can be observed via the magnitude of valley stress responses (compressive stress) of the HDA steel with increasing of fatigue cycles in Fig. 3b. However, work hardening induced in the HDA steel during strain-cyclic deformation does not give an advantageous increase in the fatigue life of CDS 1018 with aluminide coating.
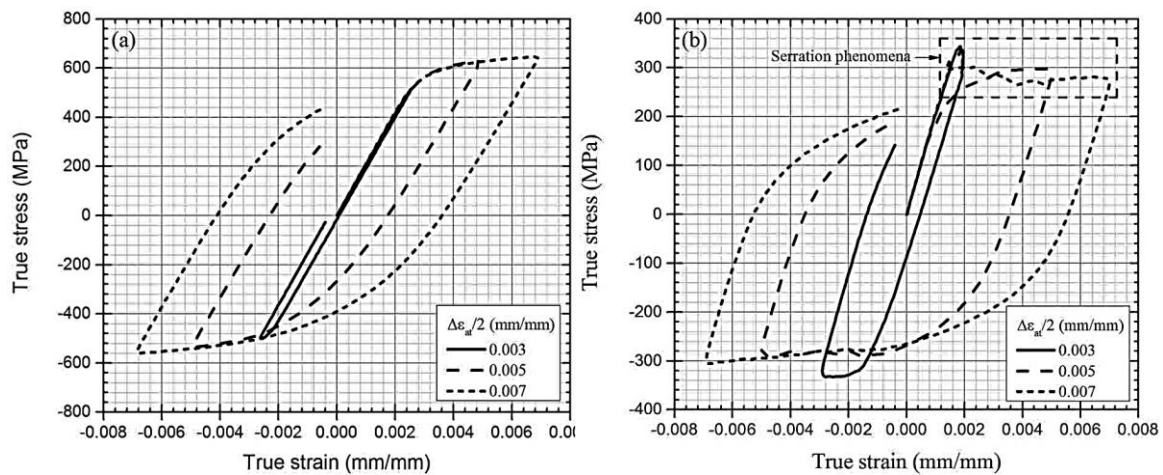
Figure 4. Hysteresis curves at the first cycle for (a) CDS 1018 steel and (b) HDA steel

3.3. Cyclic strain-stress curves analysis

The typical plot of the first hysteresis curves obtained from LCF test with the different strain amplitudes for CDS 1018 and HDA steel are depicted in Fig. 4a and b, respectively. In a strain amplitude ranging from 0.003 to 0.007 mm/mm, CDS 1018 exhibited different characteristic hysteresis loops at the first cycle (Figure 4a). In addition, CDS 1018 exhibits behaviours changes in the peak and the valley stress responses at the first cycle loading, where a valley stress response (compressive stress) is lower value than that of a peak stress response (tensile stress). This behaviours change is known as the Bauschinger effect. The strong Bauschinger effect is clearly observed in Figure 4a at any applied strain amplitudes, which is a similar characteristic with ferrite–bainite microstructures in low carbon steel [18] and an extrusion of aluminium alloy 6061-T6 [19].

Figure 4b shows the influence of the aluminide coating on CDS 1018, which significantly changes the behaviours of the steel during cyclic deformation. The HDA steel evidently shows a different stress response in tension stress at the first cycle for different strain amplitude, which yield point regions exhibited a serration characteristic. The serration phenomenon in Figure 4b is observed in the HDA steel which is a similar characteristic with the monotonic behaviours in a low carbon steel [15,16] and in an AISI 4140 steel under annealing condition [13]. The HDA steel experienced the serration phenomena of yield points at the first loading cycle can be attributed to formation of microplasticity in the Luder band region (Figure 4b). The initial microplasticity formation was as results of low dislocation interactions in the proportional yield points region and the free dislocations in this region were active [20].
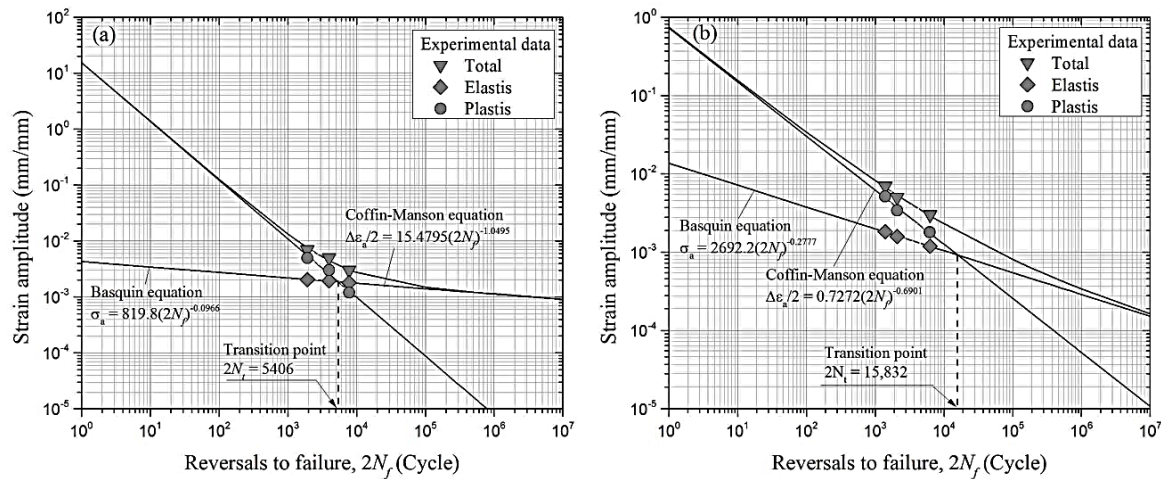
Figure 5. Plot LCF data and calibration curve obtained from the Basquin and Coffin-Manson equations for (a) CDS 1018 and (b) HDA steel

3.4. Effect of aluminide coating on the LCF properties of the steel

The relationships between a total strain amplitude ($\Delta\varepsilon_t/2$) and failure cycles ($2N_f$) are an important factor to investigate the strain-controlled fatigue life of the material due to cyclic loading. In general, the Coffin and the Manson-Basquin methods are used to determine the predictions of fatigue life of the material based on strain controlled LCF test, which is represented by the equation. (1) [12].

$$\Delta\varepsilon_t = \frac{\sigma_f'}{E}\left(2N_f\right)^b + \varepsilon_f'\left(2N_f\right)^c \tag{1}$$

Where E is elastic modulus in LCF condition (for the CDS 1018 is ~191.1 GPa and for the HDA steel is ~197.5 GPa), N_f is the fatigue life or the number of cycles to failure, σ_f' (MPa) is the fatigue strength coefficient, b is the fatigue strength exponent, ε_f' is the fatigue ductility coefficient, and c is the fatigue ductility exponent. Eq. (1) is results of combination of the elastic component and the plastic components obtained from experimental LCF tests as given by equation. (2) and (3), respectively.

$$\frac{\Delta\varepsilon_e}{2} = \frac{\sigma_f'}{E}\left(2N_f\right)^b \tag{2}$$

$$\frac{\Delta\varepsilon_p}{2} = \varepsilon_f'\left(2N_f\right)^c \tag{3}$$

Furthermore, the LCF steel's properties were determined using the curve fitting method which was similar with that of previous research [13]. The total strain versus reversal to failure cycles based on the Basquin and the Coffin-Manson equations (as the calibration curves) obtained is plotted in Fig. 5a and

8

b for the CDS 1018 and the HDA steel, respectively and the experimental data from LCF tests exhibit good correlation with the calibration curves.

The LCF resistance of metals can be represented by a value of fatigue ductility exponent [13,14,16]. In the present investigation, the fatigue ductility exponent of the HDA steel ($c = -0.6901$) is lower than that of the fatigue ductility exponent of the CDS 1018 ($c = -1.0495$), which theoretically gives a significant advantage on the LCF resistance. In addition, the high ductility of the HDA steel ($e = 46.12\%$) is possibly enable to undergo cyclic deformation but experimentally the fatigue life (N_f) of the HDA steel is lower than those the fatigue life of the CDS 1018 at all strain amplitude levels applied. In this case, the low fatigue life of the HDA steel can possibly be caused by formation of the brittle Fe_2Al_5 layer [6,8,9]. The brittle metals generally have the low plastic deformation capacity. Therefore, the Fe_2Al_5 layer was unable to resist strain cyclic deformation, which the initiation cracks were rapidly formed and propagated through this layer. Consequently, the fatigue life of the CDS 1018 with the aluminide coating under strain fatigue condition significantly decreased. The prediction of fatigue life for the CDS 1018 and the HDA steel can be determined by the elastic and plastic components using the Basquin and Coffin-Manson approach, respectively.

For the CDS 1018 steel:

$$\sigma_a = 819.8\left(2N_f\right)^{-0.0996} \tag{4}$$

$$\frac{\Delta\varepsilon_p}{2} = 15.4795\left(2N_f\right)^{-1.0495} \tag{5}$$

For the CDS 1018 steel with HDA:

$$\sigma_a = 2692.2\left(2N_f\right)^{-0.2777} \tag{6}$$

$$\frac{\Delta\varepsilon_p}{2} = 0.7272\left(2N_f\right)^{-0.6901} \tag{7}$$

The intersections between the $\Delta\varepsilon_e/2$ and $\Delta\varepsilon_p/2$ versus $2N_f$ relationship curves in Fig. 5a and b result the transition of fatigue life to reversals ($2N_t$). Furthermore, from the Eq. (4) to the Eq. (7) the number of transition cycles ($2N_t$) can be determined by substitution the values of $\varepsilon_{ae} = \varepsilon_{ap}$ and replacing $2N_f$ with $2N_t$. The number of transition cycles ($2N_t$) for the CDS 1018 and the HDA steel are 5406 cycles and 15,832 cycles, respectively. When $2N_f \gg 2N_t$, the elastic strain is more dominant to control fatigue performance of material [13]. On the contrary, when $2N_f \ll 2N_t$, the plastic strain dominantly controls the fatigue performance. In the present LCF test results, the aluminide coating applied on the CDS 1018 significantly results the high fatigue strength coefficient of the HDA steel ($\sigma_f' = 2692.2$ MPa). Therefore, the stress amplitude (σ_a) for the HDA steel can be theoretically calculated by substituting a $2N_t$ value into Eq. (6), which σ_a is an approximate 300 MPa. This recommends that the CDS 1018 with the HDA coating can safely withstand the cyclic stress at a lower stress amplitude conditions when the cyclic fatigue loading is mainly considerable in determination of an initial design for engineering components. A similar characteristic was found in the aluminide coating on K403 superalloy gas turbine

blade components, which the alloy exhibits better fatigue performance under the elastic fatigue loading than that of the fatigue performance under the plastic fatigue loading [7].

4. Conclusion

An aluminide coating on the CDS 1018 markedly reduced the mechanical strength and the strain-fatigue life of the steel. The linear-plastic behaviours of the CDS 1018 results the Bauschinger characteristic and the high ductility value of the HDA steel results the serration characteristic in yield point region. The HDA steel under high ductility condition is not capable to resist cyclically plastic deformation. The brittle Fe_2Al_5 layer on the CDS 1018 substrate was considerably believed to lead a rapid formation of initiation cracks in few cycles. A relatively high value of fatigue strength coefficient and fatigue strength exponent of the HDA steel indicate that the HDA coating applied on the CDS 1018 is appropriate for material components where the fatigue loading is the below yield strength of the material.

Acknowledgment

References
[1]   Badaruddin M, Sugiyanto and Asmi D 2019 *Mater. Res. Express* **6** 0865d6
[2]   Wang CJ and Badaruddin M 2010 *Surf. Coat. Technol*. **205** 1200
[3]   Hakam M, Wang CJ, Wardono H, Asmi D 2018 *AIP Conf. Proc*. **1983** 050002.
[4]   Badaruddin M, Sugiyanto and Asmi D 2020 *Bull. Mater. Sci*. **43** 11
[5]   Callaghan MD, Humphries SR, Law M, Ho M, Bendeich P, Li H and Yeung WY 2010 *Mater. Sci. Eng*. A **527** 5619
[6]   Aguero A, Muelas R, Gutierrez M, Vulpen RV, Osgerby S and Banks JP 2007 *Surf. Coat. Technol*. **201** 6253
[7]   Han L, Huang D, Yan X, Zhang Y, Gui M, Tao M, Zhang X and Qi M 2019 *Intl. J. Fat*. **125** 491
[8]   Dryepondt S and Pint BA 2010 *Surf. Coat. Technol*. **205** 1195
[9]   Badaruddin M, Riza RT and Zulhanif 2018 *AIP Conf. Proc*. **1983** 050004
[10]   Badaruddin M, Sugiri A and Wang CJ 2020 J. *Construction and Building Materials* **232** 117193
[11]   ASTM E8M Standard test methods for tension testing of metallic materials, ASTM International, West Conshohocken, PA, 2016
[12]   ASTM E 606-04 Standard practice for strain-controlled fatigue testing, ASTM International, West Conshohocken, PA, 2012
[13]   Badaruddin M, Sugiyanto, Wardono H, Andoko, Wang C J and Rivai A K 2019 *Intl. J. Fatigue* **125** 406.
[14]   Yang L, Gao Y, Shi G, Wang X and Bai Y 2018 *Constr. Build. Mater*. **165** 688
[15]   Fatoba O and Akid R 2018 *Theo. Appl. Frac. Mech*. **94** 147
[16]   Yu MT, DuQuesnay DL and Topper TH 1990 *Intl. J. Fat*. **15** 433
[17]   Xie X, Ning D and Sun J 2016 *Mater. Charact*. **120** 195
[18]   Smirnov MA, Pyshmintsev IY, Varnak OV, Mal′tseva AN and Goikhenberg YN 2016 *Steel in Translation* **46** 58
[19]   Badaruddin M, Zulhanif and Supriadi H 2019 *J. Phys.: Conf. Ser*. **1198** 032002
[20]   Tsuchida N, Tomota Y, Nagai K and Fukaura K 2006 *Scrip. Mater*. **54** 57